PERGAMON

International Journal of Solids and Structures 40 (2003) 5157–5174

INTERNATIONAL JOURNAL OF SOLIDS and STRUCTURES

www.elsevier.com/locate/ijsolstr

Electroelastic analysis of a piezoelectric cylindrical fiber with a penny-shaped crack embedded in a matrix

S. Lin, F. Narita, Y. Shindo *

Department of Materials Processing, Graduate School of Engineering, Tohoku University, Aoba-yama 02, Sendai 980-8579, Japan

Received 22 August 2002; received in revised form 9 January 2003

Abstract

The electroelastic response of a penny-shaped crack in a piezoelectric cylindrical fiber embedded in an elastic matrix is investigated in this study. Fourier and Hankel transforms are used to reduce the problem to the solution of a pair of dual integral equations. They are then reduced to a Fredholm integral equation of the second kind. Numerical values on the stress intensity factor, energy release rate and energy density factor for piezoelectric composites are obtained to show the influence of applied electric fields.

Keywords: Elasticity; Integral equation; Piezocomposite; Crack; Stress intensity factor; Energy release rate

1. Introduction

Mechanical reliability and durability of polymer/piezoelectric ceramic composites with 1–3 connectivity are important considerations in the design of hydrophones and transducers. In recent years, significant efforts had been made to the study of electroelastic fields concentrations and fracture behavior of 1–3 piezoelectric composites (Shindo et al., 2002a,b). In the theoretical studies of the piezoelectric crack problems, the electrical boundary condition imposed across the crack surface remains a debating issue. There are two commonly used electrical boundary conditions. Pak (1990) has assumed crack face to be free of surface charge (the so-called condition of impermeability or impermeable condition) while Shindo et al. (1990, 1997) have discarded the impermeability approximation. Recently, Narita and Shindo (2001) obtained a crack growth rate equation of a plane strain slit-like crack parallel to the edges of a narrow piezoelectric ceramic body under Mode I loading. The results indicated that under applied uniform displacement, positive electrical fields (electrical fields in poling direction) impede crack propagation while negative electrical fields (electrical fields applied opposite to the poling direction) aid crack propagation. To test the validity of such predictions, the single-edge precracked-beam tests and corresponding finite element analyses were performed on P-7 piezoelectric ceramics (Shindo et al., 2002c). For center-cracked piezoelectric

* Corresponding author. Tel./fax: +81-22-217-7341.
E-mail address: shindo@material.tohoku.ac.jp (Y. Shindo).

0020-7683/$ - see front matter © 2003 Elsevier Ltd. All rights reserved.
doi:10.1016/S0020-7683(03)00261-0

specimens under three-point bending condition, total potential and mechanical strain energy release rates based on the exact boundary condition for applied displacement are in agreement with the experimental results. However, the total and mechanical energy release rates based on the impermeable assumption are not in agreement with the experimental results. In the case of applied load, the total and mechanical energy release rates based on the exact crack model are also in agreement with the experimental results of Park and Sun (1995). Their experimental results showed that positive electric fields decreased fracture load, whereas negative electric fields increased it. The fracture mechanism is due to the inducement of stress resulting from mechanical deformation by the applied electric field. Based on the total and mechanical energy release rates for the impermeable model under applied force, we cannot explain the test results. To estimate the electric fracture toughness, indentation fracture tests were also made on P-7 under combined mechanical and electrical loads (Shindo et al., 2001). The exact crack model provided predictions of fracture properties due to electromechanical loading and better qualitative agreement with the experimental results. Schneider and Heyer (1999) also used the indentation method to determine the crack growth of ferroelectric barium titanate and showed that it is physically questionable to apply the impermeable crack model. In recent works, the energy density fracture criterion (Sih, 1991) was applied to determine the piezoelectric crack growth segments for conditions of positive, negative and zero electric field based on the impermeable assumption (Sih and Zuo, 2000).

This paper considers the electroelastic problem of a penny-shaped crack in a piezoelectric circular cylinder embedded in an elastic matrix under Mode I loading. The method of solution involves the use of Fourier and Hankel transforms to reduce the mixed boundary value problem to a pair of dual integral equations. The solution is then given in terms of a Fredholm integral equation of the second kind. The stress intensity factor, energy release rate and energy density factor are determined and numerical results are shown graphically to demonstrate the influence of applied electric fields.

2. Problem statement and basic equations

A piezoelectric fiber of infinite length with radius b in Fig. 1 is embedded in an elastic matrix having Young's modulus E and Poisson's ratio v. With the reference to a cylindrical coordinate system (r, θ, z), the longitudinal axis of the fiber coincides with the z-axis while the center of a penny-shaped crack of radius a is directed through the z-axis. The piezoelectric composite is subjected to an external strain in the z-direction, and the fiber poled in the z-direction is subjected to the normal stress, $\sigma_{zz} = \sigma_\infty$, and electric field, $E_z = E_\infty$. Quantities in the neighboring elastic matrix will subsequently be designated by the superscript 'E'.

The constitutive equations can be written as

$$\left.\begin{aligned}
\sigma_{rr} &= c_{11}u_{r,r} + c_{12}\frac{u_r}{r} + c_{13}u_{z,z} - e_{31}E_z \\
\sigma_{\theta\theta} &= c_{12}u_{r,r} + c_{11}\frac{u_r}{r} + c_{13}u_{z,z} - e_{31}E_z \\
\sigma_{zz} &= c_{13}u_{r,r} + c_{13}\frac{u_r}{r} + c_{33}u_{z,z} - e_{33}E_z \\
\sigma_{zr} &= c_{44}(u_{r,z} + u_{z,r}) - e_{15}E_r
\end{aligned}\right\} \tag{1}$$

$$\left.\begin{aligned}
D_r &= e_{15}(u_{r,z} + u_{z,r}) + \epsilon_{11}E_r \\
D_z &= e_{31}\left(u_{r,r} + \frac{u_r}{r}\right) + e_{33}u_{z,z} + \epsilon_{33}E_z
\end{aligned}\right\} \tag{2}$$

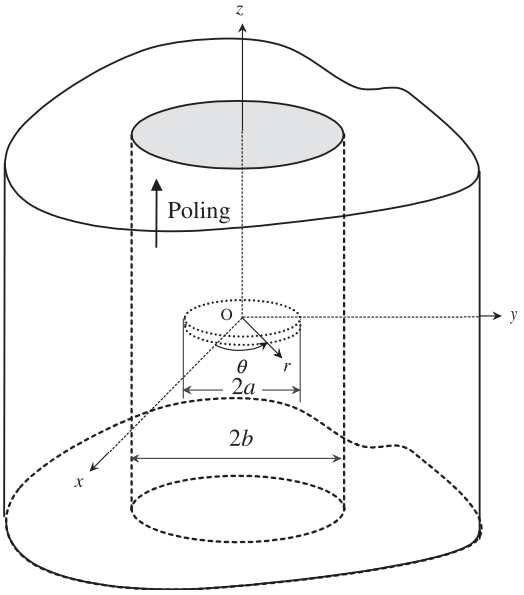

Fig. 1. Geometry of a piezoelectric cylindrical fiber with a penny-shaped crack embedded in a matrix.

$$\left.\begin{aligned}
\sigma_{rr}^{E} &= (2\mu+\lambda)u_{r,r}^{E} + \lambda\left(\frac{u_r^{E}}{r} + u_{z,z}^{E}\right)\\
\sigma_{\theta\theta}^{E} &= \lambda u_{r,r}^{E} + (2\mu+\lambda)\frac{u_r^{E}}{r} + \lambda u_{z,z}^{E}\\
\sigma_{zz}^{E} &= \lambda\left(u_{r,r}^{E} + \frac{u_r^{E}}{r}\right) + (2\mu+\lambda)u_{z,z}^{E}\\
\sigma_{zr}^{E} &= \mu(u_{r,z}^{E} + u_{z,r}^{E})
\end{aligned}\right\} \tag{3}$$

In Eqs. (1)–(3), σ_{rr}, $\sigma_{\theta\theta}$, σ_{zz}, σ_{zr}, σ_{rr}^{E}, $\sigma_{\theta\theta}^{E}$, σ_{zz}^{E}, σ_{zr}^{E} are the components of stress tensor; D_r and D_z the components of electric displacement vector; u_r, u_z, u_r^{E} and u_z^{E} the components of displacement vectors; E_r and E_z the components of electric field vector; c_{11}, c_{12}, c_{13}, c_{33}, c_{44} the elastic moduli measured in a constant electric field; ϵ_{11}, ϵ_{33} the dielectric permittivities measured at constant strain; e_{15}, e_{31}, e_{33} the piezoelectric constants; $\lambda = 2Gv/(1-2v)$ and $\mu = G$ the Lamé constants of the elastic matrix; and $G = E/2(1+v)$ the modulus of rigidity. A comma implies partial differentiation with respect to the coordinates. The electric field components may be written in terms of an electric potential $\phi(r,z)$ by

$$E_r = -\phi_{,r}, \quad E_z = -\phi_{,z} \tag{4}$$

The governing equations are obtained as

$$\left.\begin{aligned}
&c_{11}\left(u_{r,rr} + \frac{u_{r,r}}{r} - \frac{u_r}{r^2}\right) + c_{44}u_{r,zz} + (c_{13}+c_{44})u_{z,rz} + (e_{31}+e_{15})\phi_{,rz} = 0\\
&(c_{13}+c_{44})\left(u_{r,rz} + \frac{u_{r,z}}{r}\right) + c_{33}u_{z,zz} + c_{44}\left(u_{z,rr} + \frac{u_{z,r}}{r}\right) + e_{15}\left(\phi_{,rr} + \frac{\phi_{,r}}{r}\right) + e_{33}\phi_{,zz} = 0
\end{aligned}\right\} \tag{5}$$

$$(e_{31}+e_{15})\left(u_{r,rz} + \frac{u_{r,z}}{r}\right) + e_{15}\left(u_{z,rr} + \frac{u_{z,r}}{r}\right) + e_{33}u_{z,zz} - \epsilon_{11}\left(\phi_{,rr} + \frac{\phi_{,r}}{r}\right) - \epsilon_{33}\phi_{,zz} = 0 \tag{6}$$

$$\left.\begin{aligned}&(2\mu+\lambda)\left(u^{\mathrm{E}}_{r,rr}+\frac{u^{\mathrm{E}}_{r,r}}{r}-\frac{u^{\mathrm{E}}_{r}}{r^2}\right)+\mu u^{\mathrm{E}}_{r,zz}+(\mu+\lambda)u^{\mathrm{E}}_{z,rz}=0\\&(\mu+\lambda)\left(u^{\mathrm{E}}_{r,rz}+\frac{u^{\mathrm{E}}_{r,z}}{r}\right)+(2\mu+\lambda)u^{\mathrm{E}}_{z,zz}+\mu\left(u^{\mathrm{E}}_{z,rr}+\frac{u^{\mathrm{E}}_{z,r}}{r}\right)=0\end{aligned}\right\} \tag{7}$$

In a vacuum, the constitutive equations (2) and the governing equation (6) become

$$D_r=\epsilon_0 E_r,\quad D_z=\epsilon_0 E_z \tag{8}$$

$$\phi_{,rr}+\frac{\phi_{,r}}{r}+\phi_{,zz}=0 \tag{9}$$

where ϵ_0 is the electric permittivity of the vacuum.

Referring to the semi-infinite region $z\geqslant 0$, $0\leqslant r<\infty$, $0\leqslant\theta\leqslant 2\pi$, the boundary conditions can be expressed in the form

$$\begin{aligned}&\sigma_{zr}(r,0)=0\quad(0\leqslant r\leqslant b)\\&\sigma^{\mathrm{E}}_{zr}(r,0)=0\quad(b\leqslant r\leqslant\infty)\end{aligned} \tag{10}$$

$$\begin{aligned}&\sigma_{zz}(r,0)=0\quad(0\leqslant r<a)\\&u_z(r,0)=0\quad(a\leqslant r\leqslant b)\\&u^{\mathrm{E}}_z(r,0)=0\quad(b\leqslant r\leqslant\infty)\end{aligned} \tag{11}$$

$$\begin{aligned}&E_r(r,0)=E^{\mathrm{c}}_r(r,0)\quad(0\leqslant r<a)\\&\phi(r,0)=0\quad(a\leqslant r\leqslant b)\end{aligned} \tag{12}$$

$$D_z(r,0)=D^{\mathrm{c}}_z(r,0)\quad(0\leqslant r<a) \tag{13}$$

$$u_r(b,z)=u^{\mathrm{E}}_r(b,z) \tag{14}$$

$$u_z(b,z)=u^{\mathrm{E}}_z(b,z) \tag{15}$$

$$\sigma_{rr}(b,z)=\sigma^{\mathrm{E}}_{rr}(b,z) \tag{16}$$

$$\sigma_{rz}(b,z)=\sigma^{\mathrm{E}}_{rz}(b,z) \tag{17}$$

$$D_r(b,z)=0 \tag{18}$$

$$\begin{aligned}&\sigma_{zz}(r,z)=\sigma_\infty,\quad E_z(r,z)=E_\infty\quad(0\leqslant r\leqslant b,\ z\to\infty)\\&\sigma^{\mathrm{E}}_{zz}(r,z)=\sigma^{\mathrm{E}}_\infty\quad(b\leqslant r<\infty,\ z\to\infty)\end{aligned} \tag{19}$$

where

$$\begin{aligned}\sigma^{\mathrm{E}}_\infty&=c_1\sigma_\infty+(c_1e_1-e_2)E_\infty\\c_1&=\frac{(2\mu+\lambda)[2(\mu+\lambda)-c_{11}-c_{12}]-2\lambda(\lambda-c_{13})}{c_{33}[2(\mu+\lambda)-c_{11}-c_{12}]-2c_{13}(\lambda-c_{13})}\\e_1&=e_{33}+\frac{2c_{13}e_{31}}{2(\mu+\lambda)-c_{11}-c_{12}}\\e_2&=\frac{2\lambda e_{31}}{2(\mu+\lambda)-c_{11}-c_{12}}\end{aligned} \tag{20}$$

and the superscript 'c' stands for the electric field quantity in the void inside the crack. The far-field normal stress σ_∞ is expressed as

$$\sigma_\infty = \sigma_0 - e_2 E_\infty \tag{21}$$

Note that σ_0 is a uniform normal stress for a closed-circuit condition with the potential forced to remain zero (grounded).

3. Solution procedure

Assume that the solutions u_r, u_z, ϕ, u_r^{E} and u_z^{E} are of the form

$$\begin{aligned} u_r(r,z) &= \frac{2}{\pi}\sum_{j=1}^{3}\int_0^\infty [a_j A_j(\alpha)\exp(-\gamma_j \alpha z)J_1(\alpha r) + a'_j B_j(\alpha) I_1(\gamma'_j \alpha r)\cos(\alpha z)]\,\mathrm{d}\alpha + a_\infty r \\ u_z(r,z) &= \frac{2}{\pi}\sum_{j=1}^{3}\int_0^\infty \left[\frac{1}{\gamma_j}A_j(\alpha)\exp(-\gamma_j \alpha z)J_0(\alpha r) + \frac{1}{\gamma'_j}B_j(\alpha) I_0(\gamma'_j \alpha r)\sin(\alpha z)\right]\mathrm{d}\alpha + b_\infty z \end{aligned} \tag{22}$$

$$\phi(r,z) = \frac{2}{\pi}\sum_{j=1}^{3}\int_0^\infty \left[-\frac{b_j}{\gamma_j}A_j(\alpha)\exp(-\gamma_j \alpha z)J_0(\alpha r) + \frac{b'_j}{\gamma'_j}B_j(\alpha) I_0(\gamma'_j \alpha r)\sin(\alpha z)\right]\mathrm{d}\alpha - c_\infty z \tag{23}$$

$$\begin{aligned} u_r^{\mathrm{E}}(r,z) &= \frac{2}{\pi}\int_0^\infty \{-K_1(\alpha r)B_4(\alpha) + [4(1-\nu)K_2(\alpha r) + \alpha r K_0(\alpha r)]B_5(\alpha)\}\cos(\alpha z)\,\mathrm{d}\alpha + a_\infty b + d_\infty (r-b) \\ u_z^{\mathrm{E}}(r,z) &= \frac{2}{\pi}\int_0^\infty [-K_0(\alpha r)B_4(\alpha) + \alpha r K_1(\alpha r)B_5(\alpha)]\sin(\alpha z)\,\mathrm{d}\alpha + e_\infty z \end{aligned} \tag{24}$$

where $A_j(\alpha)$ $(j=1,2,3)$ and $B_j(\alpha)$ $(j=1,\ldots,5)$ are the unknowns to be solved, $J_0(\ )$ and $J_1(\ )$ are the zero and first order Bessel functions of the first kind, $I_0(\ )$ and $I_1(\ )$ are the zero and first order modified Bessel functions of the first kind, and $K_0(\ )$, $K_1(\ )$ and $K_2(\ )$ are the zero, first and second order modified Bessel functions of the second kind, respectively. The real constants a_∞, b_∞, c_∞, d_∞ and e_∞ will be determined from the far-field loading conditions, and γ_j^2, a_j, b_j, $\gamma_j'^2$, a'_j, b'_j $(j=1,2,3)$ are given in Appendix A. Application of the Fourier transform to Eq. (9) yields

$$\phi^{\mathrm{c}} = \frac{2}{\pi}\int_0^\infty C(\alpha)\sinh(\alpha z)J_0(\alpha r)\,\mathrm{d}\alpha \quad (0 \leqslant x < a) \tag{25}$$

where $C(\alpha)$ is also unknown.

By applying the far-field loading conditions, the constants a_∞, b_∞, c_∞, d_∞ and e_∞ are evaluated as

$$\begin{aligned} a_\infty = d_\infty &= \frac{(c_{13}-\lambda)\sigma_\infty + [(c_{13}-\lambda)e_{33} - c_{33}e_{31}]E_\infty}{2c_{13}(c_{13}-\lambda) - c_{33}(c_{11}+c_{12}-2\lambda-2\mu)} \\ b_\infty = e_\infty &= \frac{-(c_{11}+c_{12}-2\lambda-2\mu)\sigma_\infty + [2c_{13}e_{31} - e_{33}(c_{11}+c_{12}-2\lambda-2\mu)]E_\infty}{2c_{13}(c_{13}-\lambda) - c_{33}(c_{11}+c_{12}-2\lambda-2\mu)} \\ c_\infty &= E_\infty \end{aligned} \tag{26}$$

The boundary conditions of Eqs. (10) and (12) lead to the following relations between unknown functions:

$$\frac{f_1}{\gamma_1}A_1(\alpha) + \frac{f_2}{\gamma_2}A_2(\alpha) + \frac{f_3}{\gamma_3}A_3(\alpha) = 0 \tag{27}$$

$$\frac{b_1}{\gamma_1}A_1(\alpha)+\frac{b_2}{\gamma_2}A_2(\alpha)+\frac{b_3}{\gamma_3}A_3(\alpha)=0 \tag{28}$$

where

$$f_j=c_{44}(a_j\gamma_j^2+1)-e_{15}b_j \quad (j=1,2,3) \tag{29}$$

Application of the mixed boundary conditions in Eqs. (11) gives rise to a pair of dual integral equations:

$$\begin{aligned}&\int_0^\infty \alpha F D(\alpha)J_0(\alpha r)\,\mathrm{d}\alpha-\sum_{j=1}^{3}\int_0^\infty \alpha g_j\gamma_j B_j(\alpha)I_0(\gamma_j'\alpha r)\,\mathrm{d}\alpha=-\frac{\pi}{2}\sigma_\infty \quad (0\leqslant r<a)\\ &\int_0^\infty D(\alpha)J_0(\alpha r)\,\mathrm{d}\alpha=0 \quad (a\leqslant r\leqslant b)\end{aligned} \tag{30}$$

where

$$D(\alpha)=\frac{A_1(\alpha)}{d_1}=\frac{A_2(\alpha)}{d_2}=\frac{A_3(\alpha)}{d_3} \tag{31}$$

$$F=\sum_{j=1}^{3}d_jg_j \tag{32}$$

$$d_1=\gamma_1(b_2f_3-b_3f_2),\quad d_2=\gamma_2(b_3f_1-b_1f_3),\quad d_3=\gamma_3(b_1f_2-b_2f_1) \tag{33}$$

$$g_j=c_{13}a_j-c_{33}+e_{33}b_j \quad (j=1,2,3) \tag{34}$$

The solution of a pair of dual integral equations (30) may be obtained by using a new function $\Phi(\xi)$ and the result is

$$D(\alpha)=-\frac{\sigma_\infty}{F}a^2\int_0^1 \Phi(\xi)\sin(a\alpha\xi)\,\mathrm{d}\xi \tag{35}$$

The function $\Phi(\xi)$ is governed by the following Fredholm integral equation of the second kind:

$$\Phi(\xi)+\int_0^1 \Phi(\eta)K(\xi,\eta)\,\mathrm{d}\eta=\xi \tag{36}$$

The kernel function $K(\xi,\eta)$ is

$$K(\xi,\eta)=\frac{4}{\pi^2F}\sum_{j=1}^{3}g_j\gamma_j^2\int_0^\infty E_j(\alpha,\eta)\sinh(\gamma_j'\alpha\xi)\,\mathrm{d}\alpha \tag{37}$$

where $E_j(\alpha,\eta)$ is given in Appendix B.

The stress intensity factor k_1 for the exact crack model is obtained as

$$k_1=\lim_{r\to a^+}\{2(r-a)\}^{1/2}\sigma_{zz}(r,0)=\frac{2}{\pi}\sigma_\infty\sqrt{a}\Phi(1) \tag{38}$$

The electric displacement intensity factor k_D is also given by

$$k_\mathrm{D}=\lim_{r\to a^+}\{2(r-a)\}^{1/2}D_z(r,0)=\left(\frac{1}{F}\sum_{j=1}^{3}h_jd_j\right)k_1 \tag{39}$$

where

$$h_j = e_{31}a_j + e_{33} - \epsilon_{33}b_j \tag{40}$$

The stress and electric displacement intensity factors for the impermeable crack model are discussed in Appendix C.

By using the concept of crack closure energy and the asymptotic behavior of stresses, displacements, electric displacement and electric potential near the crack border, the total potential energy release rate G may be expressed as

$$\begin{aligned} G &= \lim_{\Delta a\to 0}\frac{1}{\Delta a}\int_0^{\Delta a}\{\sigma_{zz}(r_1)u_z(\Delta a - r_1) + \sigma_{zr}(r_1)u_r(\Delta a - r_1) + D_z(r_1)\phi(\Delta a - r_1)\}\,\mathrm{d}r_1 \\ &= -\frac{\pi}{2F^2}\left(F\sum_{j=1}^{3}\frac{d_j}{\gamma_j} - \sum_{j=1}^{3}h_j d_j\sum_{j=1}^{3}\frac{b_j d_j}{\gamma_j}\right)k_1^2 \end{aligned} \tag{41}$$

where $r_1 = \{(r-a)^2 + z^2\}^{1/2}$ and Δa is the assumed crack extension. The mechanical strain energy release rate G_{M} includes only mechanical energy released as the crack extends and is given by

$$G_{\mathrm{M}} = \lim_{\Delta a\to 0}\frac{1}{\Delta a}\int_0^{\Delta a}\{\sigma_{zz}(r_1)u_z(\Delta a - r_1) + \sigma_{zr}(r_1)u_r(\Delta a - r_1)\}\,\mathrm{d}r_1 = -\left(\frac{\pi}{2F}\sum_{j=1}^{3}\frac{d_j}{\gamma_j}\right)k_1^2 \tag{42}$$

The total potential and mechanical strain energy release rates for the impermeable crack model are also given in Appendix C.

The energy density is expressible in the form

$$\mathrm{d}W = \left\{\frac{1}{2}(\sigma_{rr}\varepsilon_{rr} + \sigma_{zr}\varepsilon_{zr} + \sigma_{rz}\varepsilon_{rz} + \sigma_{zz}\varepsilon_{zz}) + \frac{1}{2}(D_rE_r + D_zE_z)\right\}\mathrm{d}V \tag{43}$$

and hence

$$S = r_1\frac{\mathrm{d}W}{\mathrm{d}V} = (a_{\mathrm{M}} + a_{\mathrm{E}})k_1^2 \tag{44}$$

where

$$\begin{aligned} a_{\mathrm{M}} = \frac{1}{8F^2}\Bigg\{ &\sum_{j=1}^{3}m_j d_j R_j^{\mathrm{c}}(\theta_1)\sum_{j=1}^{3}a_j d_j R_j^{\mathrm{c}}(\theta_1) + \sum_{j=1}^{3}\frac{f_j d_j}{\gamma_j}R_j^{\mathrm{s}}(\theta_1)\sum_{j=1}^{3}\frac{d_j(a_j\gamma_j^2+1)}{\gamma_j}R_j^{\mathrm{s}}(\theta_1) \\ &- \sum_{j=1}^{3}g_j d_j R_j^{\mathrm{c}}(\theta_1)\sum_{j=1}^{3}d_j R_j^{\mathrm{c}}(\theta_1)\Bigg\} \end{aligned} \tag{45}$$

$$a_{\mathrm{E}} = \frac{1}{8F^2}\left\{\sum_{j=1}^{3}\frac{n_j d_j}{\gamma_j}R_j^{\mathrm{s}}(\theta_1)\sum_{j=1}^{3}\frac{b_j d_j}{\gamma_j}R_j^{\mathrm{s}}(\theta_1) - \sum_{j=1}^{3}h_j d_j R_j^{\mathrm{c}}(\theta_1)\sum_{j=1}^{3}b_j d_j R_j^{\mathrm{c}}(\theta_1)\right\} \tag{46}$$

and

$$\begin{aligned} R_j^{\mathrm{c}}(\theta_1) &= \left\{\frac{(\cos^2\theta_1 + \gamma_j^2\sin^2\theta_1)^{1/2} + \cos\theta_1}{\cos^2\theta_1 + \gamma_j^2\sin^2\theta_1}\right\}^{1/2} \\ R_j^{\mathrm{s}}(\theta_1) &= -\left\{\frac{(\cos^2\theta_1 + \gamma_j^2\sin^2\theta_1)^{1/2} - \cos\theta_1}{\cos^2\theta_1 + \gamma_j^2\sin^2\theta_1}\right\}^{1/2} \end{aligned} \tag{47}$$

$$\theta_1 = \tan^{-1}\left(\frac{z}{r-a}\right) \tag{48}$$

The energy density factor for the impermeable crack model is given in Appendix C.

Rapid crack growth occurs when the minimum energy density factor $S_{\min}$ reaches a critical value:

$$S_{\min} = S_c \tag{49}$$

Each increment of stable crack growth $r_{11}, r_{12}, \ldots, r_{1j}, \ldots, r_{1c}$ up to rapid crack propagation is determined by the condition (Sih, 1991)

$$\frac{S_1}{r_{11}} = \frac{S_2}{r_{12}} = \cdots = \frac{S_j}{r_{1j}} = \cdots = \frac{S_c}{r_{1c}} \tag{50}$$

where r_{1c} represents the last ligament of slow crack growth just prior to the onset of rapid fracture and S_c governs the onset of rapid crack propagation. The growth condition of Eq. (50) can be written as

$$\frac{S_{j-}}{r_{1j-}} = \frac{S_{j0}}{r_{1j0}} = \frac{S_{j+}}{r_{1j+}} \tag{51}$$

where the subscripts −, 0, + denote, respectively, the situations for negative, zero and positive electric fields.

4. Numerical results and discussion

The determination of the stress intensity factor, energy release rate and energy density factor for the exact crack model requires the solution of the function of $\Phi(\xi)$. The solution of the Fredholm integral equation of the second kind (36) governing $\Phi(\xi)$ has been computed numerically by the use of Gaussian quadrature formulas. Once this is done, k_1, G, G_M and S can be found from Eqs. (38), (41), (42) and (44). The simultaneous Fredholm integral equations of the second kind (C.4) were also solved numerically to yield the values of the functions $\Phi_1(1)$ and $\Phi_2(1)$. These values were then inserted into Eqs. (C.2) and (C.3) to determine the stress and electric displacement intensity factors for the impermeable crack model. The energy release rate and energy density factor were calculated by using Eqs. (C.12), (C.13) and (C.15)–(C.17). The piezoelectric cylinder is made of commercially available piezoceramic P-7, and the elastic matrix is epoxy. The material properties of P-7 are listed in Table 1 (Shindo et al., 2000). The Young's modulus and Poisson's ratio of epoxy are taken to be $E = 3.38$ GPa and $v = 0.215$.

Fig. 2 shows the normalized stress intensity factor $\pi k_1/2\sigma_0 a^{1/2}$ of the exact and impermeable (approximate) crack models as a function of the crack-radius to cylinder-radius ratio a/b for various values of the normalized electric field $e_1 E_\infty/\sigma_0$. The data are normalized by the stress intensity factor $2\sigma_0 a^{1/2}/\pi$ of an infinite P-7 piezoelectric ceramic for $E_\infty = 0$ V/m corresponding to the applied uniform displacement. For comparison, the normalized stress intensity factor $\pi k_1/2\sigma_0 a^{1/2}$ of a free surface finite P-7 piezoceramic cylinder for the exact crack model under $E_\infty = 0$ V/m is also included in the figure. An increase of a/b causes an increase in the stress intensity factor. The stress intensity factor of the P-7-epoxy composite for $E_\infty = 0$ V/m remains smaller than that of the P-7 cylinder. When an electric field is applied, $\pi k_1/2\sigma_0 a^{1/2}$ increases or decreases depending on the direction of the electric field. The stress intensity factor k_1 normalized by $2\sigma_\infty a^{1/2}/\pi$ corresponding to the applied uniform stress for the exact and impermeable

Table 1
Material properties of a piezoelectric ceramic P-7

	Elastic stiffnesses ($\times 10^{10}$ N/m^2)				Piezoelectric coefficients (C/m^2)			Dielectric constants ($\times 10^{-10}$ C/V m)	
	c_{11}	c_{33}	c_{44}	c_{13}	e_{31}	e_{33}	e_{15}	ϵ_{11}	ϵ_{33}
P-7	13.0	11.9	2.5	8.3	−10.3	14.7	13.5	171.0	186.0

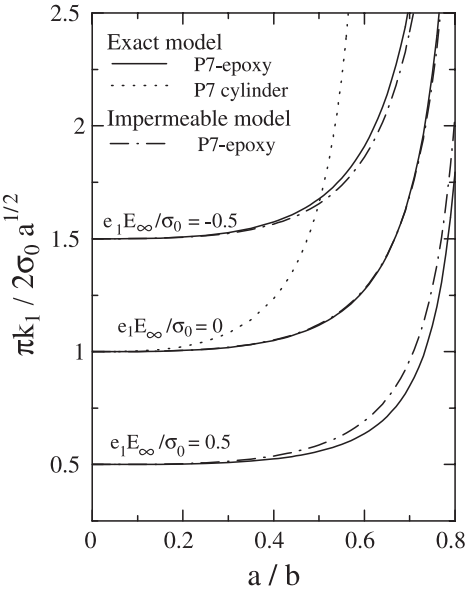

Fig. 2. Stress intensity factor versus crack-radius to cylinder-radius ratio.

crack models is independent of the normalized electric field $e_1E_\infty/\sigma_\infty$, and agrees with the $\pi k_1/2\sigma_0 a^{1/2}$ for $E_\infty = 0$ V/m.

Fig. 3 shows the dependence of the total potential energy release rate G for the exact crack model under applied displacement on e_1E_∞/σ_0 for $a/b = 0.7$, where the result has been normalized by the energy release rate G_0 of the infinite P-7 for $E_\infty = 0$ V/m. For comparison, the mechanical strain energy release rate G_M for the exact crack model, total potential energy release rate G^I and mechanical strain energy release rate G^I_M

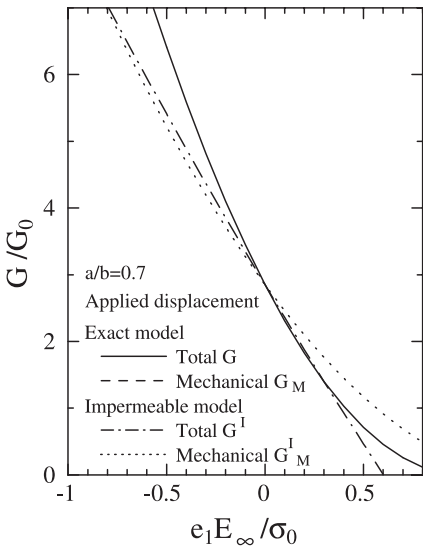

Fig. 3. Energy release rate versus electric field for applied displacement.

for the impermeable crack model are also included in the figure. Comparing the results of G and G_M, little difference is observed (solid and dashed lines approximately overlap). The total energy release rate for the exact crack model is lower for positive electric fields and higher for negative electric fields. On the other hand, when a positive electric field is larger, a negative total energy release rate is produced for the impermeable crack model (alternate long and short dashed line). It has been pointed out by at least 15 or more researchers previously (e.g. McMeeking, 1999; Chen and Lynch, 1999; Sih, 2002). The parameter for the impermeable crack model has questionable physical significance. Fig. 4 shows the energy density factor S_j (crack growth segment r_{1j}) for the exact crack model for applied displacement under different e_2E_∞/σ_0, $a/b = 0.7$ and $\theta_1 = 0$, where S_j (r_{1j}) has been normalized by the energy density factor S_{j0} (crack growth segment r_{1j0}) of the infinite P-7. Also shown are data for the impermeable crack model. The presence of positive electric field E_∞ leads to a decrease in the energy density factor (crack growth segment) for the exact crack model. In contrast, the energy density factor (crack growth segment) increases as the electric field E_∞ increases in the negative direction. For the exact boundary condition, no substantial difference is found in the effects of the electric fields on crack propagation based on the stress intensity factor, total potential energy release rate, mechanical strain energy release rate and energy density factor. The energy density factor for the impermeable crack model is higher for positive electric fields and lower for negative electric fields. This is in contrast to the total potential and mechanical strain energy release rates for the impermeable crack model. The presentation of data for the impermeable crack model causes confusion in using the electrical boundary conditions on the crack face.

Fig. 5 displays the variation of G and G_M for the exact crack model and G^I and G^I_M for the impermeable crack model under applied uniform stress with various normalized electric field $e_1E_\infty/\sigma_\infty$ for $a/b = 0.7$, normalized by values of the infinite P-7 for $E_\infty = 0$ V/m. The total potential and mechanical strain energy release rates for the exact crack model are independent of the normalized electric field $e_1E_\infty/\sigma_\infty$ (solid and dashed lines overlap). In the impermeable case, as the magnitude of $e_1E_\infty/\sigma_\infty$ is increased from zero, the total potential energy release rate G^I can be made either to increase or to decrease depending on the directions of E_∞. But, once maximum G^I is reached, further increase in E_∞ will monotonically decrease G^I,

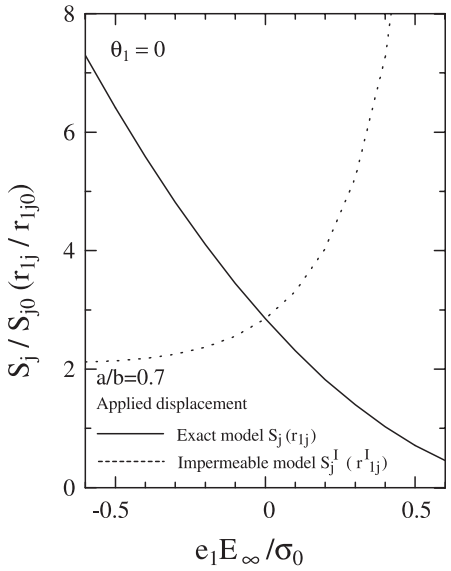

Fig. 4. Energy density factor versus electric field for applied displacement.

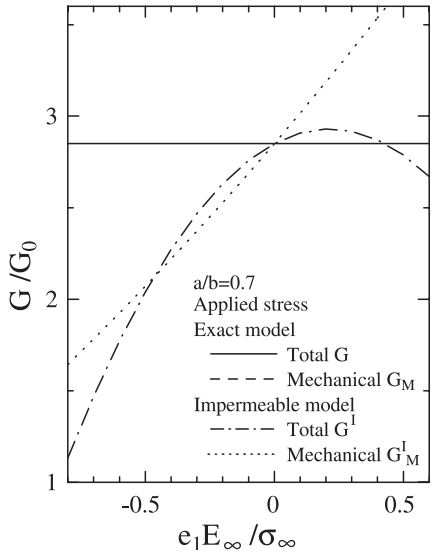

Fig. 5. Energy release rate versus electric field for applied stress.

which is inconsistent with the experimental findings. The normalized energy density factor (crack growth segment) for the exact crack model versus $e_1E_\infty/\sigma_\infty$ for $a/b = 0.7$ is presented in Fig. 6, along with the results for the impermeable crack model normalized by the corresponding values of energy density factor (crack growth segment) of the infinite P-7 for $E_\infty = 0$ V/m. The energy density factor (crack growth segment) for the exact crack model is also independent of $e_1E_\infty/\sigma_\infty$. In contrast, the energy density factor

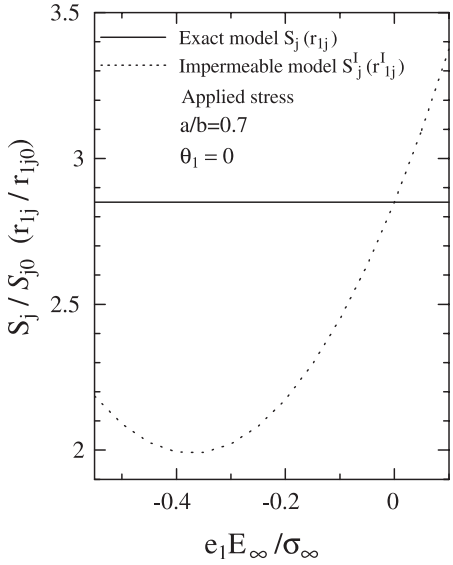

Fig. 6. Energy density factor versus electric field for applied displacement.

(crack growth segment) for the impermeable crack model increases or decreases depending on the magnitude and direction of $e_1E_\infty/\sigma_\infty$. If the impermeable crack model is used, different criteria give different results for the crack propagation in piezoelectric ceramics and composites.

5. Conclusions

The electroelastic problem of a penny-shaped crack in a piezoelectric cylindrical fiber embedded in an elastic matrix has theoretically been analyzed. The results are expressed in terms of the stress intensity factor, energy release rate and energy density factor. Fracture mechanics parameters such as stress intensity factor, energy release rate and energy density factor increase and the effect of electrical loading becomes significant as the cylinder-radius is decreased in comparison with the penny-shaped crack-radius. Fracture mechanics parameters for the 1–3 piezoelectric composite are smaller than those for the piezoelectric cylinder if the other parameters are held constant. The electrical loading dependence on the fracture mechanics parameters is different for the two mechanical loading conditions (applied displacement and applied stress). For the exact boundary condition, fracture mechanics parameters under uniform displacement are lower for positive electric fields and higher for negative electric fields. For applied stress, fracture mechanics parameters for the exact crack model are independent of the electric fields. No consensus is reached on the fracture criteria for the impermeable crack model.

Acknowledgements

This work was supported by the Ministry of Education, Culture, Sports, Science and Technology of Japan under the Grant-in-Aid for Scientific Research (B) and Grant-in-Aid for Exploratory Research.

Appendix A

γ_j^2 $(j = 1, 2, 3)$ in Eqs. (22) and (23) are the roots of the following characteristic equation:

$$a_0\gamma^6 + b_0\gamma^4 + c_0\gamma^2 + d_0 = 0 \tag{A.1}$$

where

$$\begin{aligned}
a_0 &= c_{44}(c_{33}\epsilon_{33} + e_{33}^2)\\
b_0 &= -2c_{44}e_{15}e_{33} - c_{11}e_{33}^2 - c_{33}(c_{44}\epsilon_{11} + c_{11}\epsilon_{33}) + \epsilon_{33}(c_{13} + c_{44})^2 + 2e_{33}(c_{13} + c_{44})(e_{31} + e_{15})\\
&\quad - c_{44}^2\epsilon_{33} - c_{33}(e_{31} + e_{15})^2\\
c_0 &= 2c_{11}e_{15}e_{33} + c_{44}e_{15}^2 + c_{11}(c_{33}\epsilon_{11} + c_{44}\epsilon_{33}) - \epsilon_{11}(c_{13} + c_{44})^2 - 2e_{15}(c_{13} + c_{44})(e_{31} + e_{15})\\
&\quad + c_{44}^2\epsilon_{11} + c_{44}(e_{31} + e_{15})^2\\
d_0 &= -c_{11}(c_{44}\epsilon_{11} + e_{15}^2)
\end{aligned} \tag{A.2}$$

and, $\gamma_j'^2$, a_j, b_j, a_j', b_j' $(j = 1, 2, 3)$ stand for the abbreviation

$$\gamma_j'^2 = \frac{1}{\gamma_j^2} \tag{A.3}$$

$$a_j = \frac{(e_{31}+e_{15})(c_{33}\gamma_j^2 - c_{44}) - (c_{13}+c_{44})(e_{33}\gamma_j^2 - e_{15})}{(c_{44}\gamma_j^2 - c_{11})(e_{33}\gamma_j^2 - e_{15}) + (c_{13}+c_{44})(e_{31}+e_{15})\gamma_j^2} \tag{A.4}$$

$$b_j = \frac{(c_{44}\gamma_j^2 - c_{11})a_j + (c_{13}+c_{44})}{e_{31}+e_{15}} \tag{A.5}$$

$$a'_j = -a_j\gamma_j^2 \tag{A.6}$$

$$b'_j = -b_j \tag{A.7}$$

Appendix B

The functions $E_j(\alpha,\eta)$ $(j=1,2,3)$ in Eq. (37) are given by

$$E_j(\alpha,\eta) = \sum_{i=1}^{5} \frac{D_i(\alpha,\eta)Q_{i,j}(\alpha)}{|C|} \quad (j=1,2,3) \tag{B.1}$$

where

$$C = \begin{bmatrix} c_{1,1}(\alpha) & c_{1,2}(\alpha) & c_{1,3}(\alpha) & c_{1,4}(\alpha) & c_{1,5}(\alpha) \\ c_{2,1}(\alpha) & c_{2,2}(\alpha) & c_{2,3}(\alpha) & c_{2,4}(\alpha) & c_{2,5}(\alpha) \\ c_{3,1}(\alpha) & c_{3,2}(\alpha) & c_{3,3}(\alpha) & c_{3,4}(\alpha) & c_{3,5}(\alpha) \\ c_{4,1}(\alpha) & c_{4,2}(\alpha) & c_{4,3}(\alpha) & c_{4,4}(\alpha) & c_{4,5}(\alpha) \\ c_{5,1}(\alpha) & c_{5,2}(\alpha) & c_{5,3}(\alpha) & c_{5,4}(\alpha) & c_{5,5}(\alpha) \end{bmatrix} \tag{B.2}$$

$$\begin{aligned} c_{1,j}(\alpha) &= a'_j I_1(\gamma'_j \alpha b/a) \\ c_{2,j}(\alpha) &= \gamma_j I_0(\gamma'_j \alpha b/a) \\ c_{3,j}(\alpha) &= -m_j\gamma_j \alpha I_0(\gamma'_j \alpha b/a) + \frac{b}{a}(c_{12}-c_{11}) I_1(\gamma'_j \alpha b/a) \quad (j=1,2,3) \\ c_{4,j}(\alpha) &= -f_j I_1(\gamma'_j \alpha b/a) \\ c_{5,j}(\alpha) &= -n_j I_1(\gamma'_j \alpha b/a) \end{aligned} \tag{B.3}$$

$$\begin{aligned} c_{1,4}(\alpha) &= K_1(\alpha b/a) \\ c_{2,4}(\alpha) &= K_0(\alpha b/a) \\ c_{3,4}(\alpha) &= -2\mu\left[\alpha K_0(\alpha b/a) + \frac{b}{a}K_1(\alpha b/a)\right] \\ c_{4,4}(\alpha) &= 2\mu K_1(\alpha b/a) \\ c_{5,4}(\alpha) &= 0 \end{aligned} \tag{B.4}$$

$$
\begin{aligned}
c_{1,5}(\alpha) &= -4(1-\nu)\left[K_0(\alpha b/a) + \frac{2a}{\alpha b}K_1(\alpha b/a)\right] + \frac{\alpha b}{a}K_1(\alpha b/a)\\
c_{2,5}(\alpha) &= -\frac{\alpha b}{a}K_0(\alpha b/a)\\
c_{3,5}(\alpha) &= 2\mu\frac{b}{a}\left[\left(4-4\nu+\frac{b^2\alpha^2}{a^2}\right)K_1(\alpha b/a) + (3-2\nu)\frac{\alpha b}{a}K_1(\alpha b/a)\right]\\
c_{4,5}(\alpha) &= 2\mu\left[(2-2\nu)K_1(\alpha b/a) + \frac{\alpha b}{a}K_0(\alpha b/a)\right]\\
c_{5,5}(\alpha) &= 0
\end{aligned}
\tag{B.5}
$$

$$
\begin{aligned}
D_1(\alpha,\eta) &= \sum_{j=1}^{3}\frac{a_j d_j}{\gamma_j}K_1(\gamma_j'\alpha b/a)\sinh(\gamma_j'\alpha\eta)\\
D_2(\alpha,\eta) &= \sum_{j=1}^{3}\frac{d_j}{\gamma_j^2}\left[-\frac{m_j\alpha}{\gamma_j}K_0(\gamma_j'\alpha b/a) + (c_{12}-c_{11})\frac{a_j a}{b}K_0(\gamma_j'\alpha b/a)\right]\sinh(\gamma_j'\alpha\eta)\\
D_3(\alpha,\eta) &= \sum_{j=1}^{3}\frac{d_j}{\gamma_j}K_0(\gamma_j'\alpha b/a)\sinh(\gamma_j'\alpha\eta)\\
D_4(\alpha,\eta) &= \sum_{j=1}^{3}\frac{f_j d_j}{\gamma_j^3}K_1(\gamma_j'\alpha b/a)\sinh(\gamma_j'\alpha\eta)\\
D_5(\alpha,\eta) &= \sum_{j=1}^{3}\frac{n_j d_j}{\gamma_j}K_1(\gamma_j'\alpha b/a)\sinh(\gamma_j'\alpha\eta)
\end{aligned}
\tag{B.6}
$$

$$
\begin{aligned}
m_j &= c_{11}a_j - c_{13} + e_{31}b_j\\
n_j &= e_{15}(a_j\gamma_j^2 + 1) + \epsilon_{11}b_j \quad (j=1,2,3)
\end{aligned}
\tag{B.7}
$$

and $|C|$ is the determinant of the square matrix C and $Q_{i,j}(\alpha)$ are the cofactors of the elements $c_{i,j}(\alpha)$.

Appendix C

The impermeable boundary condition becomes

$$
\begin{aligned}
D_z(r,0) &= 0 \quad (0 \leqslant r < a)\\
\phi(r,0) &= 0 \quad (a \leqslant r \leqslant b)
\end{aligned}
\tag{C.1}
$$

The boundary condition of Eq. (10) leads to Eq. (27). Making use of mixed boundary conditions of Eqs. (11) and (C.1), two simultaneous dual integral equations are obtained.

The stress intensity factor k_1 and electric displacement intensity factor k_D for the impermeable crack model are obtained as

$$
k_1 = \frac{2}{\pi}\sigma_\infty\sqrt{a}\{\Phi_1(1) + \Phi_2(1)\} \tag{C.2}
$$

$$
k_D = \frac{2}{\pi}\sigma_\infty\sqrt{a}\left\{\frac{F_{21}}{F_{11}}\Phi_1(1) + \frac{F_{22}}{F_{12}}\Phi_2(1)\right\} \tag{C.3}
$$

The functions $\Phi_1(\xi)$ and $\Phi_2(\xi)$ in Eqs. (C.2) and (C.3) are the solutions of the following simultaneous Fredholm integral equations of the second kind:

$$\begin{aligned}
&\Phi_1(\xi)+\Phi_2(\xi)+\int_0^1 \Phi_1(\eta)K_{11}(\xi,\eta)\,\mathrm{d}\eta+\int_0^1 \Phi_2(\eta)K_{12}(\xi,\eta)\,\mathrm{d}\eta=\xi\\
&\frac{F_{21}}{F_{11}}\Phi_1(\xi)+\frac{F_{22}}{F_{12}}\Phi_2(\xi)+\int_0^1 \Phi_1(\eta)K_{21}(\xi,\eta)\,\mathrm{d}\eta+\int_0^1 \Phi_2(\eta)K_{22}(\xi,\eta)\,\mathrm{d}\eta=\frac{D^*}{\sigma_\infty}\xi
\end{aligned} \tag{C.4}$$

where

$$F_{11}=\sum_{j=1}^{3} g_j d_j,\quad F_{12}=\sum_{j=1}^{3} g_j l_j,\quad F_{21}=\sum_{j=1}^{3} h_j d_j,\quad F_{22}=\sum_{j=1}^{3} h_j l_j \tag{C.5}$$

$$l_1=\gamma_1(f_2-f_3),\quad l_2=\gamma_2(f_3-f_1),\quad l_3=\gamma_3(f_1-f_2) \tag{C.6}$$

$$D^*=c_2\sigma_\infty+e_3E_\infty \tag{C.7}$$

$$\begin{aligned}
c_2&=\frac{2e_{31}(c_{13}-\lambda)-e_{33}(c_{11}+c_{12}-2\lambda-2\mu)}{2c_{13}(c_{13}-\lambda)-c_{33}(c_{11}+c_{12}-2\lambda-2\mu)}\\
e_3&=\frac{2e_{31}[(c_{13}-\lambda)e_{33}-c_{33}e_{31}]+e_{33}[2c_{13}e_{31}-e_{33}(c_{11}+c_{12}-2\lambda-2\mu)]}{2c_{13}(c_{13}-\lambda)-c_{33}(c_{11}+c_{12}-2\lambda-2\mu)}+\epsilon_{33}
\end{aligned} \tag{C.8}$$

The kernels $K_{ij}(\xi,\eta)$ $(i,j=1,2)$ are given by

$$\begin{aligned}
K_{11}(\xi,\eta)&=\frac{4}{\pi^2F}\sum_{j=1}^{3} g_j\gamma_j^2\int_0^\infty E_j(\alpha,\eta)\sinh(\gamma_j'\alpha\xi)\,\mathrm{d}\alpha\\
K_{12}(\xi,\eta)&=\frac{4}{\pi^2F}\sum_{j=1}^{3} g_j\gamma_j^2\int_0^\infty E_j'(\alpha,\eta)\sinh(\gamma_j'\alpha\xi)\,\mathrm{d}\alpha\\
K_{21}(\xi,\eta)&=\frac{4}{\pi^2F}\sum_{j=1}^{3} h_j\gamma_j^2\int_0^\infty E_j(\alpha,\eta)\sinh(\gamma_j'\alpha\xi)\,\mathrm{d}\alpha\\
K_{22}(\xi,\eta)&=\frac{4}{\pi^2F}\sum_{j=1}^{3} h_j\gamma_j^2\int_0^\infty E_j'(\alpha,\eta)\sinh(\gamma_j'\alpha\xi)\,\mathrm{d}\alpha
\end{aligned} \tag{C.9}$$

where

$$E_j'(\alpha,\eta)=\sum_{i=1}^{5}\frac{D_i'(\alpha,\eta)Q_{i,j}(\alpha)}{|C|}\quad (j=1,2,3) \tag{C.10}$$

$$
\begin{aligned}
D'_1(\alpha,\eta) &= \sum_{j=1}^{3} \frac{a_j l_j}{\gamma_j} K_1(\gamma'_j \alpha b/a)\sinh(\gamma'_j \alpha \eta) \\
D'_2(\alpha,\eta) &= \sum_{j=1}^{3} \frac{l_j}{\gamma_j^2}\left[-\frac{m_j \alpha}{\gamma_j} K_0(\gamma'_j \alpha b/a) + (c_{12}-c_{11})\frac{a_j a}{b} K_0(\gamma'_j \alpha b/a)\right]\sinh(\gamma'_j \alpha \eta) \\
D'_3(\alpha,\eta) &= \sum_{j=1}^{3} \frac{l_j}{\gamma_j} K_0(\gamma'_j \alpha b/a)\sinh(\gamma'_j \alpha \eta) \\
D'_4(\alpha,\eta) &= \sum_{j=1}^{3} \frac{f_j l_j}{\gamma_j^3} K_1(\gamma'_j \alpha b/a)\sinh(\gamma'_j \alpha \eta) \\
D'_5(\alpha,\eta) &= \sum_{j=1}^{3} \frac{n_j l_j}{\gamma_j} K_1(\gamma'_j \alpha b/a)\sinh(\gamma'_j \alpha \eta)
\end{aligned}
\tag{C.11}
$$

The total potential energy release rate G and mechanical strain energy release rate G_{M} for the impermeable crack model are

$$
\begin{aligned}
G = -\frac{\pi}{2(F_{11}F_{22}-F_{12}F_{21})^2}\Bigg\{ &\left[(F_{11}F_{22}-F_{12}F_{21})\sum_{j=1}^{3}\frac{s_j}{\gamma_j} - \sum_{j=1}^{3} h_j s_j \sum_{j=1}^{3}\frac{b_j s_j}{\gamma_j}\right] k_1^2 + \Bigg[\sum_{j=1}^{3} h_j t_j \sum_{j=1}^{3}\frac{b_j s_j}{\gamma_j} \\
&+ \sum_{j=1}^{3} h_j s_j \sum_{j=1}^{3}\frac{b_j t_j}{\gamma_j} - (F_{11}F_{22}-F_{12}F_{21})\sum_{j=1}^{3}\frac{t_j}{\gamma_j}\Bigg] k_1 k_{\mathrm{D}} - \left(\sum_{j=1}^{3} h_j t_j \sum_{j=1}^{3}\frac{b_j t_j}{\gamma_j}\right) k_{\mathrm{D}}^2 \Bigg\}
\end{aligned}
\tag{C.12}
$$

$$
G_{\mathrm{M}} = -\frac{\pi}{2(F_{11}F_{22}-F_{12}F_{21})}\left[\left(\sum_{j=1}^{3}\frac{s_j}{\gamma_j}\right)k_1^2 - \left(\sum_{j=1}^{3}\frac{t_j}{\gamma_j}\right)k_1 k_{\mathrm{D}}\right] \tag{C.13}
$$

where

$$
\begin{aligned}
s_j &= d_j F_{22} - l_j F_{21} \\
t_j &= d_j F_{12} - l_j F_{11} \quad (j=1,2,3)
\end{aligned}
\tag{C.14}
$$

The energy density factor is expressible in the form

$$
S = S_{\mathrm{M}} + S_{\mathrm{E}} \tag{C.15}
$$

where

$$
S_{\mathrm{M}} = \frac{1}{8(F_{11}F_{22}-F_{12}F_{21})^2}(\beta_1 k_1^2 + \beta_2 k_1 k_{\mathrm{D}} + \beta_3 k_{\mathrm{D}}^2) \tag{C.16}
$$

$$
S_{\mathrm{E}} = \frac{1}{8(F_{11}F_{22}-F_{12}F_{21})^2}(\beta_4 k_1^2 + \beta_5 k_1 k_{\mathrm{D}} + \beta_6 k_{\mathrm{D}}^2) \tag{C.17}
$$

and

$$
\begin{aligned}
\beta_1 &= \sum_{j=1}^{3} m_j s_j R_j^{\mathrm{c}}(\theta_1) \sum_{j=1}^{3} a_j s_j R_j^{\mathrm{c}}(\theta_1) + 2\sum_{j=1}^{3} \frac{f_j s_j}{\gamma_j} R_j^{\mathrm{s}}(\theta_1) \sum_{j=1}^{3} \frac{s_j(a_j\gamma_j^2+1)}{\gamma_j} R_j^{\mathrm{s}}(\theta_1) \\
&\quad - \sum_{j=1}^{3} g_j s_j R_j^{\mathrm{c}}(\theta_1) \sum_{j=1}^{3} s_j R_j^{\mathrm{c}}(\theta_1) \\
\beta_2 &= -\sum_{j=1}^{3} m_j t_j R_j^{\mathrm{c}}(\theta_1) \sum_{j=1}^{3} a_j s_j R_j^{\mathrm{c}}(\theta_1) - 2\sum_{j=1}^{3} \frac{f_j t_j}{\gamma_j} R_j^{\mathrm{s}}(\theta_1) \sum_{j=1}^{3} \frac{s_j(a_j\gamma_j^2+1)}{\gamma_j} R_j^{\mathrm{s}}(\theta_1) \\
&\quad + \sum_{j=1}^{3} g_j t_j R_j^{\mathrm{c}}(\theta_1) \sum_{j=1}^{3} s_j R_j^{\mathrm{c}}(\theta_1) - \sum_{j=1}^{3} m_j s_j R_j^{\mathrm{c}}(\theta_1) \sum_{j=1}^{3} a_j t_j R_j^{\mathrm{c}}(\theta_1) \\
&\quad - 2\sum_{j=1}^{3} \frac{f_j s_j}{\gamma_j} R_j^{\mathrm{s}}(\theta_1) \sum_{j=1}^{3} \frac{t_j(a_j\gamma_j^2+1)}{\gamma_j} R_j^{\mathrm{s}}(\theta_1) + \sum_{j=1}^{3} g_j s_j R_j^{\mathrm{c}}(\theta_1) \sum_{j=1}^{3} t_j R_j^{\mathrm{c}}(\theta_1) \\
\beta_3 &= \sum_{j=1}^{3} m_j t_j R_j^{\mathrm{c}}(\theta_1) \sum_{j=1}^{3} a_j t_j R_j^{\mathrm{c}}(\theta_1) + 2\sum_{j=1}^{3} \frac{f_j t_j}{\gamma_j} R_j^{\mathrm{s}}(\theta_1) \sum_{j=1}^{3} \frac{t_j(a_j\gamma_j^2+1)}{\gamma_j} R_j^{\mathrm{s}}(\theta_1) \\
&\quad - \sum_{j=1}^{3} g_j t_j R_j^{\mathrm{c}}(\theta_1) \sum_{j=1}^{3} t_j R_j^{\mathrm{c}}(\theta_1) \\
\beta_4 &= \sum_{j=1}^{3} \frac{n_j s_j}{\gamma_j} R_j^{\mathrm{s}}(\theta_1) \sum_{j=1}^{3} \frac{b_j s_j}{\gamma_j} R_j^{\mathrm{s}}(\theta_1) - \sum_{j=1}^{3} h_j s_j R_j^{\mathrm{c}}(\theta_1) \sum_{j=1}^{3} b_j s_j R_j^{\mathrm{c}}(\theta_1) \\
\beta_5 &= -\sum_{j=1}^{3} \frac{n_j t_j}{\gamma_j} R_j^{\mathrm{s}}(\theta_1) \sum_{j=1}^{3} \frac{b_j s_j}{\gamma_j} R_j^{\mathrm{s}}(\theta_1) + \sum_{j=1}^{3} h_j t_j R_j^{\mathrm{c}}(\theta_1) \sum_{j=1}^{3} b_j s_j R_j^{\mathrm{c}}(\theta_1) \\
&\quad - \sum_{j=1}^{3} \frac{n_j s_j}{\gamma_j} R_j^{\mathrm{s}}(\theta_1) \sum_{j=1}^{3} \frac{b_j t_j}{\gamma_j} R_j^{\mathrm{s}}(\theta_1) + \sum_{j=1}^{3} h_j s_j R_j^{\mathrm{c}}(\theta_1) \sum_{j=1}^{3} b_j t_j R_j^{\mathrm{c}}(\theta_1) \\
\beta_6 &= \sum_{j=1}^{3} \frac{n_j t_j}{\gamma_j} R_j^{\mathrm{s}}(\theta_1) \sum_{j=1}^{3} \frac{b_j t_j}{\gamma_j} R_j^{\mathrm{s}}(\theta_1) - \sum_{j=1}^{3} h_j t_j R_j^{\mathrm{c}}(\theta_1) \sum_{j=1}^{3} b_j t_j R_j^{\mathrm{c}}(\theta_1)
\end{aligned}
\tag{C.18}
$$

References

Chen, W., Lynch, C.S., 1999. Finite element analysis of cracks in ferroelectric ceramic materials. Engng Fract. Mech. 64, 539–562.

McMeeking, R.M., 1999. Crack tip energy release rate for a piezoelectric compact tension specimen. Engng Fract. Mech. 64, 217–244.

Narita, F., Shindo, Y., 2001. Mode I crack growth rate for yield strip model of a narrow piezoelectric ceramic body. Theor. Appl. Fract. Mech. 36, 73–85.

Pak, Y.E., 1990. Crack extension force in a piezoelectric material. ASME J. Appl. Mech. 57, 647–653.

Park, S.B., Sun, C.T., 1995. Fracture criteria for piezoelectric ceramics. J. Am. Ceram. Soc. 78, 1475–1480.

Schneider, G.A., Heyer, V., 1999. Influence of the electric field on Vickers indentation crack growth in $BaTiO_3$. J. Eur. Ceram. Soc. 19, 1299–1306.

Shindo, Y., Ozawa, E., Nowacki, J.P., 1990. Singular stress and electric fields of a cracked piezoelectric strip. Int. J. Appl. Electromag. Mater. 1, 77–87.

Shindo, Y., Tanaka, K., Narita, F., 1997. Singular stress and electric fields of a piezoelectric ceramic strip with a finite crack under longitudinal shear. Acta Mech. 120, 31–45.

Shindo, Y., Watanabe, K., Narita, F., 2000. Electroelastic analysis of a piezoelectric ceramic strip with a central crack. Int. J. Engng Sci. 38, 1–19.

Shindo, Y., Oka, M., Horiguchi, K., 2001. Analysis and testing of indentation fracture behavior of piezoelectric ceramics under an electric field. ASME J. Engng Mater. Tech. 123, 293–300.

Shindo, Y., Moribayashi, H., Narita, F., 2002a. Scattering of antiplane shear waves by a circular piezoelectric inclusion embedded in a piezoelectric medium subjected to a steady-state electrical load. Z. Angew. Math. Mech. 82, 43–49.

Shindo, Y., Minamida, K., Narita, F., 2002b. Antiplane shear wave scattering from two curved interface cracks between a piezoelectric fiber and an elastic matrix. Smart Mater. Struct. 11, 534–540.

Shindo, Y., Murakami, H., Horiguchi, K., Narita, F., 2002c. Evaluation of electric fracture properties of piezoelectric ceramics using the finite element and single-edge precracked-beam methods. J. Am. Ceram. Soc. 85 (5), 1243–1248.

Sih, G.C., 1991. Mechanics of Fracture Initiation and Propagation. Kluwer Academic Publishers, The Netherlands.

Sih, G.C., 2002. A field model interpretation of crack initiation and growth behavior in ferroelectric ceramics: change of poling direction and boundary condition. Theor. Appl. Fract. Mech. 38, 1–14.

Sih, G.C., Zuo, J.Z., 2000. Multiscale behavior of crack initiation and growth in piezoelectric ceramics. Theor. Appl. Fract. Mech. 34, 123–141.